On the role of anisotropic viscosity for plate-scale flow

T. W. Becker[1] and H. Kawakatsu[2]

[1]   We study the role of partial melt- or lattice fabric-induced, viscous anisotropy for lithosphere-asthenosphere interactions using mantle flow models. Mechanical anisotropy has only a moderate influence on plate-scale flow and global geoid predictions for the cases considered, and anisotropic weakening effects are similar to those due to effective, isotropic viscosity reduction. While anisotropy modifies details of mantle flow and may be relevant for time-dependent scenarios, it may be safely ignored for a range of other studies. These findings increase our confidence in previous isotropic modeling. They also imply that melt-rich layers may be a dynamically valid explanation for the lithosphere-asthenosphere boundary, as far as our anisotropic models are applicable. **Citation:** Becker, T. W., and H. Kawakatsu (2011), On the role of anisotropic viscosity for plate-scale flow, *Geophys. Res. Lett.*, *38*, L17307, doi:10.1029/ 2011GL048584.

1.   Introduction

[2]   Mantle convection involves fluid flow where resistance to shear is controlled by viscosity. Part of the complexity of the mantle system indeed arises from variations in viscosity, e.g., as a function of grain-size, temperature, or volatile content. What has received relatively scarce attention is the anisotropy, i.e., directional dependence, of viscosity. Such mechanical anisotropy may arise due to aligned composites of weak and strong material (shape preferred orientation, SPO, e.g., of partial melt) and/or lattice preferred orientation fabrics (LPO, e.g., of olivine with different slip system strengths), as extensively discussed in the context of seismic anisotropy [e.g., *Long and Becker*, 2010].

[3]   Viscous anisotropy is fairly well explored for ice flows [e.g., *Mangeney et al.*, 1996], but the subject is less well covered for the mantle. Early work showed that alignment of weak layers may stabilize relatively longer wavelengths of convection [*Honda*, 1986]. Using two-dimensional (2D) numerical experiments, *Christensen* [1987] found that post-glacial rebound, geoid response, and convective planforms could all be affected by anisotropic viscosity. However, *Christensen* [1987] also concluded that time-dependent convection, as opposed to steady-state situations, may lead to averaging of SPO or LPO, and overall negligible effects of mechanical anisotropy. *Han and Wahr* [1997] evaluated the role of anisotropic viscosity for postglacial rebound further and concluded that the trade-off between isotropic and anisotropic viscosity variations may make it hard to distinguish between the two.

[1]Department of Earth Sciences, University of Southern California, Los Angeles, California, USA.
[2]Ocean Hemisphere Research Center, Earthquake Research Institute, University of Tokyo, Tokyo, Japan.

[4]   More recently, *Mühlhaus et al.* [2002] explored the role of mechanical layering for folding instabilities. *Lev and Hager* [2008] argued that mechanical anisotropy should be accounted for in Rayleigh-Taylor instability theory as well as in mantle wedge temperature estimates [*Lev and Hager*, 2011], and *Tommasi et al.* [2009] tested mechanical anisotropy in the context of lithospheric deformation. Those previous studies notwithstanding, the effect of anisotropy for plate-scale flow remains largely unresolved, and no global models including anisotropic viscosity exist, to our knowledge.

[5]   Here, we study mechanical anisotropy in the astheno-sphere using 2D and global, 3D models. We only discuss instantaneous flow where the existence of anisotropy of a particular type, strength, and orientation is assumed, for simplicity. Melt-rich layers, or other compositional layering, may be relevant for a range of plate-asthenosphere interactions [*Holtzman and Kendall*, 2010] with dynamic consequences yet to be explored. In particular, we are motivated by findings that the depth of the lithosphere-asthenosphere boundary (see, e.g., *Fischer et al.* [2010] for a definition) underneath oceanic plates may be seafloor-age dependent [*Kumar and Kawakatsu*, 2011]. Such results have been interpreted as being due to SPO of partial melt underneath the thermal boundary layer [*Kawakatsu et al.*, 2009]. The *Kawakatsu et al.* "millefeuille", melt-lubrication model may also explain part of the radial seismic anisotropy which is pronounced underneath regions such as the central Pacific [*Ekström and Dziewonski*, 1998] and typically attributed to LPO of olivine under dislocation creep [*Becker et al.*, 2008].

2.   Methods

[6]   We assume that mantle flow is in the incompressible, infinite Prandtl number regime where conservation of momentum is expressed as the Stokes equation. For a given constitutive law, there is an instantaneous solution given mechanical boundary conditions and body forces.

[7]   The equations are solved numerically using the finite element codes CitcomCU [*Moresi and Solomatov*, 1995; *Zhong et al.*, 1998] for 2D and CitcomS [*Zhong et al.*, 2000; *Tan et al.*, 2006] for 3D. For our simplified 2D computations, we use a uniform resolution of 2048×512 elements for a $x \times z = 5280 \times 1320$ km domain intended to approximate the upper mantle (Figure 1). A background viscosity, ν_0, is used for the entire domain except for an asthenosphere whose isotropic viscosity, ν_a, and thickness, W, is varied. We show results with free-slip boundary conditions and lithosphere-slab anomaly driven flow, but we also explored a range of more geometrically simplified, density-driven and prescribed motion scenarios.

[8]   Additionally, a global circulation approach is used to model more realistic plate motions, mantle flow, and the geoid [e.g., *Hager*, 1984; *Ricard et al.*, 1984]. Density for these models is inferred from seismic tomography and the general setup is very similar to the best-fit models of *Ghosh*
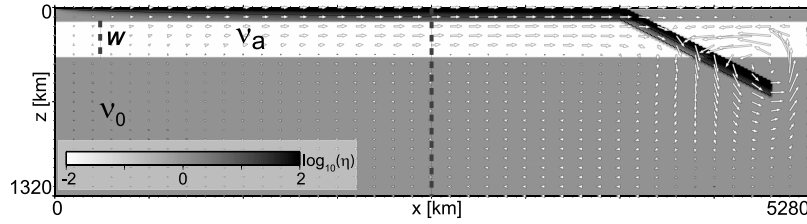
Figure 1. Velocity (vectors) and viscosity (background) for a 2D model with isotropic viscosity reduction of $\nu_a/\nu_0 = 0.01$ from $z = 100$ km to $z = 100 + W$ km with $W = 250$ km. Dashed line at $x = 2640$ km indicates the profile location as used for Figure 2. Flow is driven by lithospheric density only; temperature follows half-space cooling (limited to maximum thickness of ~100 km) from the ridge ($x = 0$) to $x = 3960$ km where the plate "subducts", as can be seen in the viscosity field, adjusted such that $\nu_{slab}/\nu_0 \approx 500$ at all depths.

et al. [2010], but at higher numerical resolution of ~20 km [*Faccenna and Becker*, 2010]. Flow is computed with a free slip surface condition and prescribed weak zones in which the lithospheric viscosity of $150\nu_0$ is reduced by a factor of 0.01 [cf. *Zhong et al.*, 2000]. The reference model has lateral viscosity variations below the lithosphere, and a factor 60 viscosity increase at 660 km depth. We study variations in the asthenospheric viscosity, with W fixed to 200 km, approximating the regions where LPO due to dislocation creep [*Becker et al.*, 2008], or SPO due to melting [*Kawakatsu et al.*, 2009], may affect flow.

[9] We modified the original codes by addition of routines that can handle a constitutive law $\tau = 2\,\mathbf{C}\dot{\epsilon}$, where τ and $\dot{\epsilon}$ are the deviatoric stress and strain-rate tensors, respectively, and $\mathbf{C}$ is the fourth-order viscosity tensor. We implemented two simplified versions of the normalized $\hat{\mathbf{C}}$, $\mathbf{C} = \nu_a\hat{\mathbf{C}}$, where the ν_a is a reference viscosity (here the asthenosphere's) and $\hat{\mathbf{C}}$ the identity matrix for isotropy. First, we used the layered fluid approximation of *Mühlhaus et al.*'s [2002] equation (8), as coded by *Moresi et al.* [2003], where $\hat{\mathbf{C}}$ can be computed based on ν_a and a layer viscosity, ν_w, for shear parallel to the (weak) plane, here expressed as $\Delta = \nu_w/\nu_a$, and the normal vector ("director") $\vec{n}$ on that plane [cf. *Christensen*, 1987].

[10] Second, we implemented the transversely isotropic, incompressible fluid of *Han and Wahr* [1997], where $\hat{\mathbf{C}}$ is obtained for a rotational symmetry axis with orientation $\vec{t}$. If $\vec{t}$ is oriented in the Cartesian z direction, then $\tau_{xy} = 2\nu_a\dot{\epsilon}_{xy}$ and $\tau_{zi} = 2\nu_w\dot{\epsilon}_{zi}$ with $i = \{x,y\}$. Transverse isotropy additionally allows for differences in pure-shear type viscosities (η_1 and $\eta_2 = 2(\eta_1 + \nu_a - \nu_w)$ [*Han and Wahr*, 1997, equation 5]), which leads to a third parameter, $\Gamma = \eta_1/\nu_a$. Here, we assume $\Gamma = 0$, for simplicity. In this case, $\Delta = 1$ corresponds to isotropy for both laws, and $\Delta \in (0; 1)$ to a preferred shear within the weakness, $\vec{n}$-plane in the case of the layered fluid, and along the symmetry axis $\vec{t}$ for transverse isotropy.

[11] The magnitudes of mechanical anisotropy in nature are somewhat uncertain, but are generally expected to be smaller for LPO ($\Delta = \mathcal{O}(0.01 \dots 0.1)$) than for SPO type ($\Delta = \mathcal{O}(0.001 \dots 0.01)$), where the latter is strongly affected by the degree of alignment and connectivity of the melt [*Takei and Holtzman*, 2009].

3. Results

3.1. Idealized, 2D Plate-Flow Models

[12] We explored a range of viscous models for the asthenosphere, varying W, ν_a, and layered and transversely

isotropic viscosity models for values of $\Delta \in [0.001, 0.1]$. Figure 2 shows horizontal velocity, v_x, against depth, z, computed for the middle of the box where flow is most plate (simple-shear) like. We only show results for the "subduction" scenario of Figure 1, but other, more geometrically simple, density-driven models yielded analogous results.

[13] Figure 2a is for an isotropic asthenosphere with $\nu_a/\nu_0 = 0.01$, for three W values as indicated. With increasing layer thickness, the horizontal flow is channeled into the asthenosphere, making the mantle lead the plate locally for $W = 250$ km (cf. Figure 1). This transition to pipe flow because of more favorable partitioning of viscous dissipation is typically facilitated by increased W or decreased ν_a/ν_0 [cf. *Hoink and Lenardic*, 2010]. Flow with kinematic boundary conditions imposes relative lithospheric motions, and decreasing ν_a in this case leads to return flow that is progressively focused entirely within the asthenosphere.

[14] If, alternatively, the asthenosphere is assumed to be of the layered anisotropic kind with $\nu_a/\nu_0 = 1$, $\Delta = 0.01$, and $\vec{n}$ oriented in z direction, overall flow is similar to the isotropic case (Figure 2b). However, return flow ($v_x < 0$) is shifted toward the bottom of the box, and the depth distribution of strain-rates in the asthenosphere is different. Shear is always concentrated at larger depths. For $\Delta = 0.001$ and $W \gtrsim 150$ km, two shear layers develop, with strain-rates again larger at the base of the asthenosphere.

[15] Partial melt induced anisotropy may be expected to be largest right underneath the thermal boundary layer [*Kawakatsu et al.*, 2009]. To mimic this behavior, we increase $\Delta(z)$ for the layered fluid of Figure 2b from $\Delta = 0.01$ at the top of the asthenosphere to $\Delta = 1$ at the bottom. If $\nu_a = \nu_0$, the flow is similar to Figure 2b; therefore, Figure 2c shows a slightly more complicated case with $\nu_a/\nu_0 = 0.1$ in addition to the depth-dependent anisotropy. This "SPO" anisotropy shows a mixture of the flow fields expected based on the previous two cases. Comparing Figures 2a and 2c, it is apparent that shear is more concentrated at shallower depths for SPO. Resulting effects in nature may, e.g., include the partitioning between dislocation and diffusion creep and hence LPO formation. While this might potentially be detected with seismic anisotropy, the trade-offs between isotropic ν_a variations and Δ are large.

[16] Figure 2d shows an "LPO" case, roughly approximated by a transversely isotropic model with $\Gamma = 0$ and $\Delta = 0.01$ where the symmetry axes, $\vec{t}$, are locally aligned with the fluid velocity, for simplicity (iterating the velocity solution until convergence to within 4% of the RMS is achieved). Real LPO-induced viscous anisotropy will clearly be more complex [e.g., *Chastel et al.*, 1993; *Tommasi et al.*, 2009],
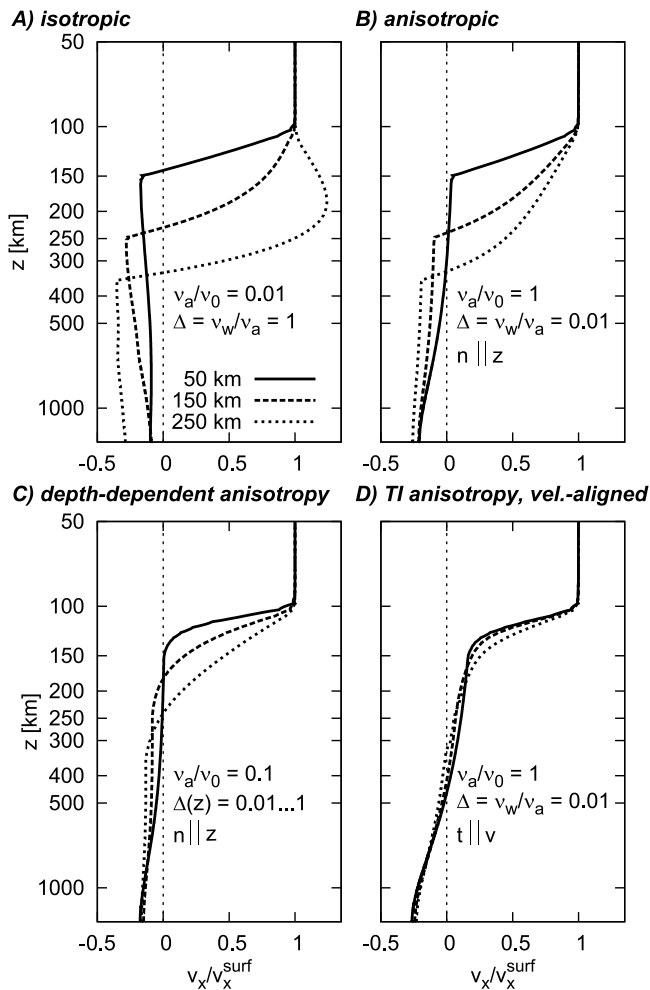
Figure 2. Horizontal velocity, v_x, normalized by the surface velocity, v_x^{surf}, as a function of depth, z, at $x = 2640$ km (Figure 1), on a semi-logarithmic scale for four rheological models and three different layer widths, W, each. (a) Isotropic viscosity reduction $\nu_a/\nu_0 = 0.01$ ($W = 250$ km case shown in Figure 1). (b) Anisotropic (layered) fluid with $\Delta = 0.01$ and $\vec{n}$ in z-direction. (c) SPO ("partial melt") model, like Figure 2b but with Δ increasing from 0.01 at $z = 100$ km to unity at $z = 100 + W$ km and $\nu_a/\nu_0 = 0.1$. (d) "LPO" model with transversely isotropic fluid, $\Delta = 0.01$, $\Gamma = 0$, and $\vec{t}$ aligned with velocities.

but Figure 2d provides a flavor of the effect of symmetry axes being non-uniformly aligned throughout the model. Expectedly, the details of the flow patterns are most different to the cases A–C in regions of up and downwellings, where flow is actually deflected out of horizontal [cf. *Lev and Hager*, 2011]. Even in the center of the plate, the velocity profile is modified, however, showing reduced shear compared to the layered fluid case at the same Δ (cf. Figures 2b and 2d). This is because the average viscosity of the anisotropic medium with irregularly aligned symmetry axes is relatively less reduced than for cases A–C. Even with $\Delta = 0.001$, the simplified "LPO" anisotropy shows less focusing than the idealized cases.

3.2. Global Circulation Models

[17] The 2D tests indicate that viscous anisotropy may affect plate-scale flow less than isotropic viscosity varia-

tions. We conducted a range of global circulation models to explore if this is borne out, focusing on surface velocities and geoid anomalies for different asthenospheric rheologies. The reference of Figure 3a is based on a model from *Ghosh et al.* [2010], modified to have a global asthenospheric viscosity reduction of $\nu_a/\nu_0 = 0.01$, for consistency with the 2D tests. While we are not concerned with optimizing the match to geoid or plate motions, we note that model A has a fairly poor fit to the geoid (correlation $r = 0.44$) which is improved to $r = 0.77$ for $\nu_a/\nu_0 = 0.1$. This reflects the well known sensitivity of the geoid to isotropic viscosity [e.g., *Hager*, 1984; *Ricard et al.*, 1984] and the perhaps less well known observation that both plate motions and the geoid can be fit well when lateral variations of viscosity are incorporated [*Ghosh et al.*, 2010]. If the isotropic viscosity reduction is limited to sub-oceanic regions (Figure 3b), the geoid is modified significantly. Velocity directions are similar to the reference, but oceanic plates are sped up compared to the continental ones [cf. *Becker*, 2006].

[18] If we consider a uniform, layered fluid anisotropy with $\Delta = 0.001$ (not shown), the geoid is very similar to Figure 3a ($r_A = 0.96$) and plate motions are near-identical to the reference case because most flow in the asthenosphere is horizontal. We get a near-perfect ($r \approx 1$) match between anisotropic and isotropic predictions by combining a $\nu_a/\nu_0 = 0.1$ reduction with $\Delta = 0.1$ for an appropriate average viscosity [cf. *Lev and Hager*, 2008]. The partial melt, SPO-inspired case with a focusing of anisotropy underneath the lithosphere (depth-dependent Δ, Figure 3c) yields a larger geoid effect than the constant Δ case, though still moderate ($r_A = 0.93$). The transverse isotropy ("LPO") case with $\vec{t}$-velocity alignment and $\Delta = 0.01$ (not shown) is visually similar to Figure 3c, but matches the reference only at $r_A = 0.68$ ($r_A^v = 0.99$, $r = 0.78$). This significant difference from case A is, however, mainly due to the effectively smaller, isotropic viscosity reduction. The geoid correlation of the LPO case with an isotropic $\nu_a/\nu_0 = 0.1$ model is 0.98.

[19] While global differences in patterns are therefore only moderate, there are regional variations between anisotropic and isotropic models (Figure 3d). The magnitude of geoid modifications (such as a flipped anomaly sign over Tibet) due to anisotropy are comparable to restricting an isotropic asthenosphere to sub-oceanic regions, and effects such as a shift of the geoid pattern close to convergent margins because of flow deflection [cf. *Christensen*, 1987] are observed.

4. Discussion

[20] Our results confirm earlier suggestions for a significant trade-off between isotropic and anisotropic viscosity variations [e.g., *Han and Wahr*, 1997]. This trade-off makes it hard to detect anisotropic effects within the asthenosphere where we expect additional, isotropic viscosity variations due to the temperature-pressure dependence of viscosity, partial melting, dissolved volatiles, or combined effects of all three.

[21] Melt-rich layer, lubrication models of the SPO type are potentially more mechanically anisotropic than LPO models but their oriented weakness gets masked by plate-scale, simple shear flow. The upside of this negative result is that models invoking partial melt for the origin of the lithosphere-asthenosphere boundary may well be dynamically consistent with a range of constraints such as the geoid.
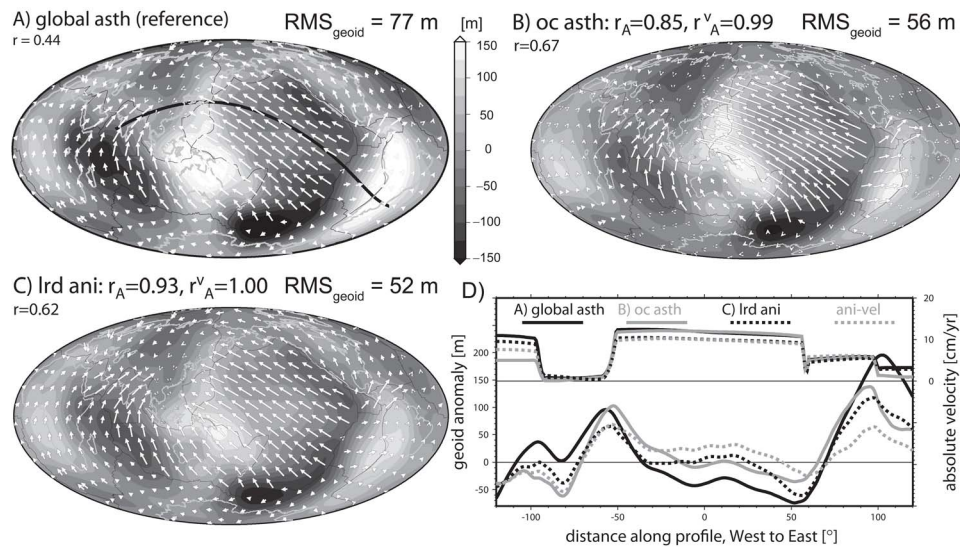
Figure 3. Geoid anomaly (RMS in legend) and surface velocities for global circulation models. (a) Reference with global, isotropic viscosity reduction between 100 and 300 km ($\nu_a/\nu_0 = 0.01$, $\Delta = \nu_w/\nu_a = 1$). (b) Viscosity reduction limited to sub-oceanic regions ($\nu_a/\nu_0 = 0.01$ sub-oceanic, $\Delta = 1$). (c) Depth-dependent, layered fluid anisotropy ("SPO"), with Δ increasing from 0.001 at 100 km to unity at 300 km ($\nu_a/\nu_0 = 1$, $\Delta(z) = 0.01 \ldots 1$, $\vec{n} \parallel \vec{r}$). Sub-plot titles show geoid, r_A, and surface velocity, r_A^v, correlation with Figure 3a), up to spherical harmonic degree $\ell = 63$; subtitles show correlation, r, with the actual geoid up to $\ell = 31$ (computed as by *Ghosh et al.* [2010]). (d) (top) Velocity and (bottom) geoid anomaly along the profile shown in Figure 3a, for models A-C and a transversely isotropic fluid ("LPO") case ($\nu_a/\nu_0 = 1$, $\Delta = 0.01$, $\Gamma = 0$, $\vec{t} \parallel \vec{v}$, cf. Figure 2d). Isotropic and anisotropic cases shown with solid and dotted lines, respectively.

[22] LPO models with more complex alignment of preferred axes lead to more interesting variations compared to isotropy, although the averaging effect due to non-uniformly oriented weak axes pointed out by *Christensen* [1987] does indeed reduce the overall role of anisotropy, and the intrinsic anisotropy is also expected to be less than for SPO.

[23] One of the major limitations of our study is that we only considered a few instantaneous flow examples for which the influence of anisotropy may overall be negligible. This only indirectly addresses more complex, evolving scenarios such as changes in plate motions, or plate boundary dynamics, where mechanical anisotropy may well be relevant.

5. Conclusions

[24] Mechanical anisotropy from the alignment of partial melt or lattice preferred fabrics has a small effect on instantaneous flow predictions beyond that which can be mimicked by isotropic viscosity variations. This emphasizes the role of lateral viscosity variations, validates a range of previous studies based on isotropic viscosity, and implies that partial melt lithosphere lubrication is a valid (though regrettably somewhat stealth) dynamic scenario.

References

Becker, T. W. (2006), On the effect of temperature and strain-rate dependent viscosity on global mantle flow, net rotation, and plate-driving forces, *Geophys. J. Int.*, *167*, 943–957.

Becker, T. W., B. Kustowski, and G. Ekström (2008), Radial seismic anisotropy as a constraint for upper mantle rheology, *Earth Planet. Sci. Lett.*, *267*, 213–237.

Chastel, Y. B., P. R. Dawson, H.-R. Wenk, and K. Bennett (1993), Anisotropic convection with implications for the upper mantle, *J. Geophys. Res.*, *98*, 17,757–17,771.

Christensen, U. R. (1987), Some geodynamical effects of anisotropic viscosity, *Geophys. J. R. Astron. Soc.*, *91*, 711–736.

Ekström, G., and A. M. Dziewonski (1998), The unique anisotropy of the Pacific upper mantle, *Nature*, *394*, 168–172.

Faccenna, C., and T. W. Becker (2010), Shaping mobile belts by small-scale convection, *Nature*, *465*, 602–605.

Fischer, K. M., D. L. Ford, H. A. Abt, and C. A. Rychert (2010), The lithosphere-asthenosphere boundary, *Ann. Rev. Earth Planet. Sci.*, *38*, 551–575.

Ghosh, A., T. W. Becker, and S. J. Zhong (2010), Effects of lateral viscosity variations on the geoid, *Geophys. Res. Lett.*, *37*, L01301, doi:10.1029/2009GL040426.

Hager, B. H. (1984), Subducted slabs and the geoid: constraints on mantle rheology and flow, *J. Geophys. Res.*, *89*, 6003–6015.

Han, D., and J. Wahr (1997), An analysis of anisotropic mantle viscosity, and its possible effects on post-glacial rebound, *Phys. Earth Planet. Inter.*, *102*, 33–50.

Hoink, T., and A. Lenardic (2010), Long wavelength convection, Poiseuille-Couette flow in the low-viscosity asthenosphere and the strength of plate margins, *Geophys. J. Int.*, *180*, 23–33.

Holtzman, B. K., and J.-M. Kendall (2010), Organized melt, seismic anisotropy, and plate boundary lubrication, *Geochem. Geophys. Geosyst.*, *11*, Q0AB06, doi:10.1029/2010GC003296.

Honda, S. (1986), Strong anisotropic flow in a finely layered asthenosphere, *Geophys. Res. Lett.*, *13*, 1454–1457.

Kawakatsu, H., P. Kumar, Y. Takei, M. Shinohara, T. Kanazawa, E. Araki, and K. Suyehiro (2009), Seismic evidence for sharp lithosphere-asthenosphere boundaries of oceanic plates, *Science*, *324*, 499–502.

Kumar, P., and H. Kawakatsu (2011), Imaging the seismic lithosphere-asthenosphere boundary of the oceanic plate, *Geochem. Geophys. Geosyst.*, *12*, Q01006, doi:10.1029/2010GC003358.

Lev, E., and B. H. Hager (2008), Rayleigh-Taylor instabilities with anisotropic lithospheric viscosity, *Geophys. J. Int.*, *173*, 806–814.

Lev, E., and B. H. Hager (2011), Anisotropic viscosity changes subduction zone thermal structure, *Geochem. Geophys. Geosyst.*, *12*, Q04009, doi:10.1029/2010GC003382.

Long, M. D., and T. W. Becker (2010), Mantle dynamics and seismic anisotropy, *Earth Planet. Sci. Lett.*, *297*, 341–354.

Mangeney, A., F. Califano, and O. Castelnau (1996), Isothermal flow of an anisotropic ice sheet in the vicinity of an ice divide, *J. Geophys. Res.*, *101*, 28,189–28,204.

Moresi, L. N., and V. S. Solomatov (1995), Numerical investigations of 2D convection with extremely large viscosity variations, *Phys. Fluids*, *7*, 2154–2162.

Moresi, L. N., F. Dufour, and H.-B. Mühlhaus (2003), A Lagrangian integration point finite element method for large deformation modeling of viscoelastic geomaterials, *J. Comput. Phys.*, *184*, 476–497.

Mühlhaus, H.-B., L. Moresi, B. Hobbs, and F. Dufour (2002), Large amplitude folding in finely layered viscoelastic rock structures, *Pure Appl. Geophys.*, *159*, 2311–2333.

Ricard, Y., L. Fleitout, and C. Froidevaux (1984), Geoid heights and lithospheric stresses for a dynamic Earth, *Ann. Geophys.*, *2*, 267–286.

Takei, Y., and B. K. Holtzman (2009), Viscous constitutive relations of solid-liquid composites in terms of grain boundary contiguity: 3. Causes and consequences of viscous anisotropy, *J. Geophys. Res.*, *114*, B06207, doi:10.1029/2008JB005852.

Tan, E., E. Choi, P. Thoutireddy, M. Gurnis, and M. Aivazis (2006), GeoFramework: Coupling multiple models of mantle convection within a computational framework, *Geochem. Geophys. Geosyst.*, *7*, Q06001, doi:10.1029/2005GC001155.

Tommasi, A., M. Knoll, A. Vauchez, J. W. Signorelli, C. Thoraval, and R. Logé (2009), Structural reactivation in plate tectonics controlled by olivine crystals anisotropy, *Nat. Geosci.*, *2*, 423–427.

Zhong, S., M. Gurnis, and L. Moresi (1998), Role of faults, nonlinear rheology, and viscosity structure in generating plates from instantaneous mantle flow models, *J. Geophys. Res.*, *103*, 15,255–15,268.

Zhong, S., M. T. Zuber, L. Moresi, and M. Gurnis (2000), Role of temperature-dependent viscosity and surface plates in spherical shell models of mantle convection, *J. Geophys. Res.*, *105*, 11,063–11,082.

T. W. Becker, Department of Earth Sciences, University of Southern California, 3651 Trousdale Pkwy., Los Angeles, CA 90089, USA. (twb@usc.edu)

H. Kawakatsu, Ocean Hemisphere Research Center, Earthquake Research Institute, University of Tokyo, 1-1-1 Yayoi, Bunkyo-ku, Tokyo 113-0032, Japan.